Article

Application of WKB Theory to Investigating Electron Tunneling in Kek-Y Graphene

Andrii Iurov *, Liubov Zhemchuzhna, Godfrey Gumbs, Danghong Huang

Posted Date: 27 April 2023

doi: 10.20944/preprints202304.1054.v1

Keywords: WKB approximation; semi-classical action; electron tunneling; transmission amplitude

 doi:10.20944/preprints202304.1054.v1

Article

Application of WKB Theory to Investigating Electron Tunneling in Kek-Y Graphene

Andrii Iurov [1,*], Liubov Zhemchuzhna [1,2], Godfrey Gumbs [2,3] and Danhong Huang [4]

1 Department of Physics and Computer Science, Medgar Evers College of City University of New York, Brooklyn, NY 11225, USA
2 Department of Physics and Astronomy, Hunter College of the City University of New York, 695 Park Avenue, New York, NY 10065, USA
3 Donostia International Physics Center (DIPC), P de Manuel Lardizabal, 4, 20018 San Sebastian, Basque Country, Spain
4 Space Vehicles Directorate, US Air Force Research Laboratory, Kirtland Air Force Base, New Mexico 87117, USA
* Correspondence: aiurov@mec.cuny.edu or theorist.physics@gmail.com

Abstract: In this paper, we have constructed a WKB approximation for graphene having a Y-shaped Kekulé lattice distortion and a special folding of the K and K' valleys, which leads to very specific linear energy dispersions with two non-equivalent pairs of subbands. These obtained semi-classical results, which include the action, electron momentum and wave functions, are utilized to analyze the dynamics of electron tunneling through non-square potential barriers. In particular, we explore resonant scattering of an electron by a potential barrier built on Kekulé-distorted graphene. Mathematically, a group of consecutive equations for a semi-classical action have been solved by following a perturbation approach under the condition of small strain-induced coupling parameter $\Delta_0 \ll 1$ (a good fit to its actual value $\Delta_0 \backsim 0.1$). Specifically, we consider a generalized model for Kek-Y graphene with two arbitrary Fermi velocities. The dependence of the electron transmission amplitude on the potential profile $V(x)$ and band parameters of Kekulé-patterned graphene has been explored and analyzed in details.

Key words: WKB approximation; semi-classical action; electron tunneling; transmission amplitude

1. Introduction

Kekulé-patterned graphene represents an unusual and technologically very promising modification of conventional graphene energy band structure due to coupling of its orbital with spin degrees of freedom. In fact, a periodic Y-shape modification of the bond strengths of graphene, as illustrated in Figure 1, leads to chiral electronic states as well as two inequivalent coupled Dirac cones with different Fermi velocities [1–3]. Practically, such a unique feature can be realized by depositing graphene on a special copper-based substrate [4]. Here, we focus on Kek-Y graphene which is further distinguished from Kek-O graphene by a finite bandgap [4–6].

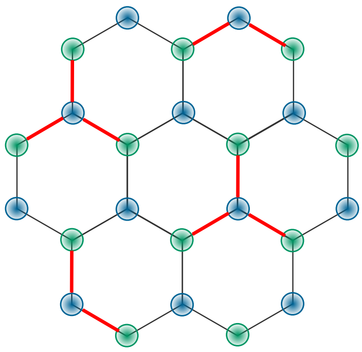

Figure 1. (Color online) Atomic structure of Kekulé-distorted grpahene: honeycomb lattices of graphene with additional Kek-Y bond texture due to the presence of a substrate.

The most crucial feature of Kek-Y graphene is its valley-momentum locking, e.g.,, two eigenstate modes of electrons are chiral (helical) and have zero bandgap, and meantime, both sublattice pseudospin and isospin are locked to the same group velocity [1]. Recently, there have been a number of crucial research publications aimed at addressing these unusual electronic, optical and transport properties of Kekulé-distorted graphene [3,7–10]. Even though the mismatch between slopes of two Dirac cones appears fixed in Kekul e-patterned graphene, i.e., $v_{F,1}/v_{F,2} \backsim 0.9$, we still consider a general case for Kek-Y graphene with two inequivalent Dirac cones and having two arbitrary Fermi velocities $v_{F,1}$ and $v_{F,2}$.

Kekulé-patterned graphene is the newest member in the family of Dirac-cone materials, including graphene [11,12], silicene [13–15], transition-metal dichalcogenides [16,17], as well as the most unusual group of α-$\mathcal{T}_3$ materials [18–20]. The most uncommon feature of α-$\mathcal{T}_3$ model is the presence of a flat band in its energy dispersions giving rise to the most unusual electronic and optical properties [21–34]. On the other hand, the magnetic properties and magnetic-quantization behavior of α-$\mathcal{T}_3$ materials have also attracted a lot of attention [35–39], including a phase transition from a diamagnetic to a paramagnetic susceptibility by continuously varying the parameter α [40]. Actually, the low-energy dispersion of α-$\mathcal{T}_3$ model looks somewhat like that of generalized Kek-Y graphene model if the Fermi velocity of the lower Dirac cone is greatly reduced compared to the larger one (i.e., $v_{F,2} \ll v_{F,1}$).

The Wentzel–Kramers–Brillouin (WKB), or the semi-classical, theory provides an intuitive but realistic description for dynamical behaviors of electrons in a variety of complex quantum systems under the condition of a high-kinetic energy. For this case, the properties of such electrons are not very much different from their classical counterparts and could be effectively described by classical dynamics. However, in contrast to a perturbation theory, the interaction between a particle and an external potential can be very strong, implying that in a number of cases the WKB description can still be valid even as other types of approximation fail [41–46]. Therefore, from this point of view, it is essential and crucial to develop a semi-classical WKB theory for each newly discovered Dirac lattice, such as α-$\mathcal{T}_3$ or Kekulé-patterned graphene. Mathematically, the WKB approximation is regarded as a solution technique for a differential equation with the highest-order derivative term multiplied by a small parameter. In quantum physics, this small parameter is just Planck's constant $\hbar$ so that the solution for a WKB wave function can be sought as a power series of $\hbar$. However, the WKB for Dirac electrons in graphene is found drastically different from that in the case of a regular Schrödinger electron, and therefore we expect that the WKB solution for each novel Dirac material will be quite unique compared with all other known solutions. Moreover, the sought wave function for a new material will usually appear as a quickly oscillating function which is further modulated by a much slower variation from an external potential $V(x)$.

Among multiple applications of the WKB theory, we would also like to calculate electron transmission, or tunneling probability, and investigate various bound states of an electronic system [44,45,47]. In contrast to previous studies on tunneling and transport of electrons in Kek-Y graphene [48,49] through complicated numerical computations, WKB methods, on the other hand, provides reliable estimates based on closed-form analytical expressions which are easily used to interpret experimental measurements on electron transport.

Studying electron tunneling, often associated with calculating a transmission amplitude, becomes one of the most important issues for each of newly discovered Dirac materials mostly because of the so-called Klein paradox, i.e., a full tunneling of chiral Dirac electrons through a square potential barrier, independent of its width and height if the incoming electron moves in the direction perpendicular to the barrier boundary [12,50–52]. For a finite-angle collision, however, a complete transmission also appears for an oblique (not a normal) incidence due to presence of Fabry-Perot resonances. Such a Klein-tunneling behavior was investigated for all Dirac-cone materials and nano-ribbons [49,53,54], including transport in Kekulé-distorted graphene nanoribbons [49]. Specifically, a magic transmission was demonstrated for α-$\mathcal{T}_3$ materials and dice lattice [55–58], in additional to unusual tunneling behavior of anisotropic Dirac electrons [59–61].

Preprints (www.preprints.org) | NOT PEER-REVIEWED | Posted: 27 April 2023 doi:10.20944/preprints202304.1054.v1

The unique properties of electron tunneling and the existence of the Klein paradox will depend on a few factors and the most crucial one is the energy bandgap between the valence and conduction bands [62–66]. The two-dimensional materials with a gap do not show Klein tunneling. Such a bandgap in graphene and other Dirac lattices could be created by applying an off-resonance circularly-polarized dressing field which also turns these material into Haldane-like Chern insulators [67,68]. However, a linearly-polarized irradiation normally does not affect the gap although it can induce or modify the existing anisotropy [69,70]. Interestingly, the effects of these external fields with different polarizations could further mix with anisotropic and tilted energy dispersions of lattices, such as $1T'MoS_2$ [71–73].

One of the most crucial applications of WKB equations is investigating the electron tunneling for non-trivial potential barriers, such as trapezoidal barriers [74] or linearly increasing potentials without a sharp boundary. It was demonstrated for all previously known Dirac materials that the Klein paradox persists in such potential profiles. Verification of this property for Kekulé-patterned graphene is one of the goals of the present paper. Since Dirac electrons moving under a linearly-increasing potential can acquire a very large kinetic energy, applying WKB approximation to such a case seems to be the most adequate and efficient approach.

The remaining part of our paper is organized as follows. We begin with a brief review of electronic states and their energy dispersions of Kek-Y graphene in Section 2. In Section 3, we formulate a full WKB approximation for a general case of Kek-Y graphene, which includes finding the semi-classical action, longitudinal electron momentum and WKB wave functions. Section 4 focuses on addressing the electron tunneling and Klein paradox in Kekulé-patterned graphene by utilizing our derived Wentzel–Kramers–Brillouin equations. Meantime, we also consider different methods for calculating electron transmissions through different types of potential barriers, and demonstrate how these methods could be applied to Kekulé-patterned graphene. Finally, we discuss and compare the obtained results and present concluding remarks in Section 5

2. Energy band structure and electronic states in Kek-Y graphene

At the outset, we briefly review the electronic band structure and eigenfunctions in Kek-Y graphene. For the type of distortion displayed in Figure 1, the Dirac cones will fold on each other, as seen in Figure 2, which results in two states with no bandgap, but with different Fermi velocities.

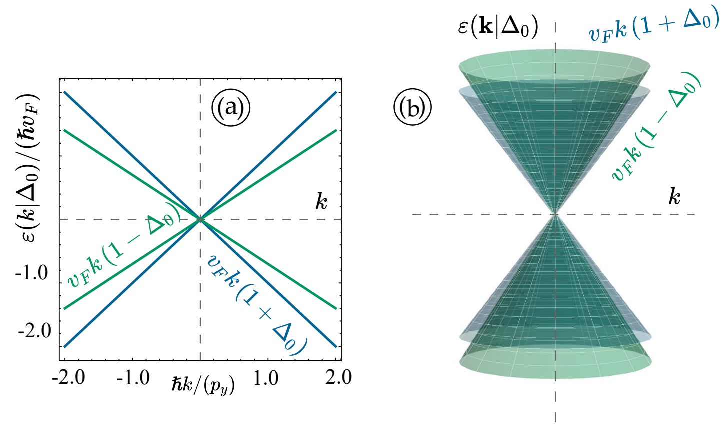

Figure 2. (Color online) Energy dispersions $\varepsilon_Y(s_1, s_2\,|\,k, \Delta_0)$ for Kek-Y graphene represented by two inequivalent Dirac cones with different Fermi velocities $v_{F,1}$ and $v_{F,2}$ corresponding to $v_F(1 \pm \Delta_0)$. Here $s_1 = \pm 1$ is a band index while $s_2 = \pm 1$ corresponds to two different Fermi velocities due to strain coupling Δ_0.

The low-energy Hamiltonian for Kek-Y graphene can be approximately written as [1,3]

$$\mathcal{H}_Y(\boldsymbol{k}\,|\,\Delta_0) = \hbar v_F \hat{\mathcal{T}}_0^{(2)} \otimes \left(\boldsymbol{k} \cdot \hat{\boldsymbol{\Sigma}}^{(2)}\right) + \hbar v_F\, \Delta_0 \left(\boldsymbol{k} \cdot \hat{\boldsymbol{\mathcal{T}}}^{(2)}\right) \otimes \hat{\Sigma}_0^{(2)}\,, \tag{1}$$

Preprints (www.preprints.org) | NOT PEER-REVIEWED | Posted: 27 April 2023 doi:10.20944/preprints202304.1054.v1

where $\boldsymbol{k} = \{k_x, k_y\}$ is a wave vector of electrons, v_F is the Fermi velocity in regular non-strained graphene and Δ_0 is a dimensionless strain-induced coupling parameter. As $\Delta_0 \to 0$, we recover the regular graphene Hamiltonian for unfolded $\boldsymbol{K}$ and $\boldsymbol{K}'$ valleys, i.e., keeping only the first term on the right hand side of Equation (1). We indicate that Equation (1) holds only for a small strain-coupling parameter Δ_0, and it may be modified as the stain strength increases. In most cases, however, Δ_0 is always assumed small in order to retain graphene signature of the system. Here, we choose $\Delta_0 \backsim 0.1$ in our calculations below but derive a generalized model by assuming a substantial difference between two Fermi velocities $v_F\,(1 \pm \Delta_0)$.

Additionally,

$$\hat{\Sigma}_x^{(2)} = \hat{\mathcal{T}}_x^{(2)} = \begin{bmatrix} 0 & 1 \\ 1 & 0 \end{bmatrix}, \tag{2}$$

$$\hat{\Sigma}_y^{(2)} = \hat{\mathcal{T}}_y^{(2)} = \begin{bmatrix} 0 & -i \\ i & 0 \end{bmatrix}, \tag{3}$$

which act in the spin- and pseudo-spin subspaces, respectively. Correspondingly, $\hat{\Sigma}_0^{(2)}$ and $\hat{\mathcal{T}}_0^{(2)}$ in Equation (1) are two 2×2 unit matrices in the spin- and pseudo-spin subspaces, written as

$$\hat{\Sigma}_0^{(2)} = \hat{\mathcal{T}}_0^{(2)} = \begin{bmatrix} 1 & 0 \\ 0 & 1 \end{bmatrix}. \tag{4}$$

Equation (1) is presented by using a Kronecker product of two 2×2 matrices, defined as

$$\overleftrightarrow{A} \otimes \overleftrightarrow{B} = \begin{bmatrix} a_{11}\overleftrightarrow{B} & a_{12}\overleftrightarrow{B} \\ a_{21}\overleftrightarrow{B} & a_{22}\overleftrightarrow{B} \end{bmatrix}. \tag{5}$$

More specifically, for the case of Pauli matrices, we have

$$\hat{\Sigma}_z^{(2)} \otimes \hat{\mathcal{T}}_z^{(2)} = \begin{bmatrix} 1 & 0 & 0 & 0 \\ 0 & -1 & 0 & 0 \\ 0 & 0 & -1 & 0 \\ 0 & 0 & 0 & 1 \end{bmatrix}, \tag{6}$$

$$\hat{\Sigma}_0^{(2)} \otimes \hat{\mathcal{T}}_z^{(2)} = \begin{bmatrix} 1 & 0 & 0 & 0 \\ 0 & -1 & 0 & 0 \\ 0 & 0 & 1 & 0 \\ 0 & 0 & 0 & -1 \end{bmatrix}. \tag{7}$$

Therefore, any block-diagonal (b-d) matrix can be built by following this procedure, i.e.,,

$$\overleftrightarrow{M}_{\text{b-d}} = \hat{\Sigma}_0^{(2)} \otimes \overleftrightarrow{A} = \left[\begin{array}{cc|cc} a_{11} & a_{12} & 0 & 0 \\ a_{21} & a_{22} & 0 & 0 \\ \hline 0 & 0 & a_{11} & a_{12} \\ 0 & 0 & a_{21} & a_{22} \end{array}\right]. \tag{8}$$

As a result, Equation (1) can take a simple matrix form

$$\hat{\mathcal{H}}_Y(\boldsymbol{k}\,|\,\Delta_0) = \hbar v_F \begin{bmatrix} \boldsymbol{k}\cdot\hat{\boldsymbol{\Sigma}}^{(2)} & \Delta_0\,(k_x - ik_y)\,\hat{\Sigma}_0^{(2)} \\ \Delta_0\,(k_x + ik_y)\,\hat{\Sigma}_0^{(2)} & \boldsymbol{k}\cdot\hat{\boldsymbol{\Sigma}}^{(2)} \end{bmatrix}, \tag{9}$$

Preprints (www.preprints.org) | NOT PEER-REVIEWED | Posted: 27 April 2023 doi:10.20944/preprints202304.1054.v1

or explicitly,

$$\mathcal{H}_Y(\boldsymbol{k}\,|\,\Delta_0) = \hbar v_F \left[\begin{array}{cc|cc} 0 & k_x + ik_y & \Delta_0(k_x - ik_y) & 0 \\ k_x - ik_y & 0 & 0 & \Delta_0(k_x - ik_y) \\ \hline \Delta_0(k_x + ik_y) & 0 & 0 & k_x + ik_y \\ 0 & \Delta_0(k_x + ik_y) & k_x - ik_y & 0 \end{array}\right] . \tag{10}$$

The energy dispersions of Kekulé-Y graphene are simply obtained as eigenvalues of the matrix defined in Equation (10), yielding

$$\varepsilon_Y(s_1, s_2\,|\,k, \Delta_0) = \hbar v_F\,(s_1 + s_2\,\Delta_0)\,k\,, \tag{11}$$

which represent two Dirac cones with different Fermi velocities $v_F(1 \pm \Delta_0)$, as displayed in Figure 2, where $s_1 = \pm 1$ is a band index while $s_2 = \pm 1$ corresponds to two different Fermi velocities due to strain coupling. These two types of subbands are often referred to as "fast" ($s_2 = +1$) and "slow" ($s_2 = -1$) Dirac cones, and importantly, photo-induced electronic transitions are allowed between these two.

In correspondence with energy dispersions in Equation (11), the normalized wave functions are calculated as

$$\Psi_Y(s_1, s_2\,|\,\boldsymbol{k}, \Delta_0) = \frac{1}{2}\begin{bmatrix} \mathrm{e}^{-i\theta_{\mathbf{k}}} \\ s_1 \\ s_2 \\ s_1 s_2\,\mathrm{e}^{+i\theta_{\mathbf{k}}} \end{bmatrix} , \tag{12}$$

where $\theta_{\mathbf{k}} = \tan^{-1}(k_y/k_x)$ is the angle associated with the electron wave vector $\boldsymbol{k}$ with respect to the x axis. The wave function in Equation (12) consists of two sub-spinors corresponding to standard graphene eigenstates, i.e.,

$$\Psi_Y(s_1, s_2\,|\,\boldsymbol{k}, \Delta_0) = \frac{1}{2}\left[\begin{array}{c} \Psi_g(s_1\,|\,\boldsymbol{k}) \\ \hline s_2\,\mathrm{e}^{+i\theta_{\mathbf{k}}}\,\Psi_g(s_1\,|\,\boldsymbol{k}) \end{array}\right] = \frac{1}{2}\left[\begin{array}{c} \begin{bmatrix} 1 \\ s_1\,\mathrm{e}^{+i\theta_{\mathbf{k}}} \end{bmatrix} \\ \hline s_2\,\mathrm{e}^{+i\theta_{\mathbf{k}}} \begin{bmatrix} 1 \\ s_1\,\mathrm{e}^{+i\theta_{\mathbf{k}}} \end{bmatrix} \end{array}\right] . \tag{13}$$

Quantum-mechanically, the velocity operators $\hat{V}_x$ for an electron can be determined by the Heisenberg equation, that is

$$\hat{V}_x \equiv \frac{d\hat{x}}{dt} = \frac{1}{i\hbar}\left[\hat{x}, \hat{\mathcal{H}}_Y(\boldsymbol{k}\,|\,\Delta_0)\right] , \tag{14}$$

which relates to an intraband probability current density $\hat{J}_x(s_1, s_2\,|\,\boldsymbol{k}, \Delta_0)$, where $\mathcal{H}_Y(\boldsymbol{k}\,|\,\Delta_0)$ is presented in Equation (9). Semi-classically, on the other hand, we define another particle velocity v_x, determined by

$$v_x = \frac{1}{\hbar}\,\frac{\partial\langle\mathcal{H}_Y(\boldsymbol{k}\,|\,\Delta_0)\rangle_{\mathrm{av}}}{\partial k_x} , \tag{15}$$

which relates to an intraband transport current density $j_x = n_0 v_x$, where n_0 is the areal density of electrons in our system while $\langle\cdots\rangle_{\mathrm{av}}$ denotes a quantum-mechanical average with respect to the wave function $\Psi_Y(s_1, s_2\,|\,\boldsymbol{k}, \Delta_0)$ presented in Equation (13).

Generally, from the Schrödinger equation, we know that the intraband probability-current density can be calculated by

$$J_x(s_1, s_2\,|\,\boldsymbol{k}, \Delta_0) \approx \left(\frac{v_F}{k_F}\right)\,\mathrm{Im}\left[\Psi^*\frac{\partial}{\partial x}\Psi\right] = v_x\,|\Psi_Y(s_1, s_2\,|\,\boldsymbol{k}, \Delta_0)|^2 , \tag{16}$$

Preprints (www.preprints.org) | NOT PEER-REVIEWED | Posted: 27 April 2023 doi:10.20944/preprints202304.1054.v1

where we treat a Kekulé particle as a free one. The definition in Equation (15) can be employed for calculating the semi-classical transport current density, yielding

$$j_x(s_1,s_2\,|\,\boldsymbol{k},\Delta_0) = n_0 v_x = n_0 v_F\left[\hat{\mathcal{T}}_0^{(2)}\otimes\hat{\Sigma}_x^{(2)}+\Delta_0\right)\left(\boldsymbol{k}\cdot\hat{\boldsymbol{\mathcal{T}}}_x^{(2)}\right)\otimes\hat{\Sigma}_0^{(2)}\Big] \tag{17}$$

$$= n_0 v_F\left[\begin{array}{cc|cc} 0 & 1 & \Delta_0 & 0 \\ 1 & 0 & 0 & \Delta_0 \\ \hline \Delta_0 & 0 & 0 & 1 \\ 0 & \Delta_0 & 1 & 0 \end{array}\right]. \tag{18}$$

An expression similar to Equation (17) should also be obtained for transport current $\hat{j}_y(s_1,s_2\,|\,\boldsymbol{k},\Delta_0)$.

For a Kekule particle, besides the intraband probability current density $\hat{\boldsymbol{J}}(s_1,s_2\,|\,\boldsymbol{k},\Delta_0)$, there exists another interband probability current density due to Δ_0 (strain) coupling between two Dirac-cones [75]. By including this interband probability current, the total particle current should be continuous and satisfies the following particle-number conversation law, i.e.,

$$\nabla\cdot\boldsymbol{J}(s_1,s_2\,|\,\boldsymbol{k},\Delta_0)+\frac{\partial}{\partial t}\left|\Psi_Y(s_1,s_2\,|\,\boldsymbol{k},\Delta_0)\right|^2=0\,. \tag{19}$$

Since there are no external sources for the current and each observable quantity is time-independent, every term in Equation (19) equals to zero, leading to

$$\frac{d}{dx}\,J_x(s_1,s_2\,|\,\boldsymbol{k},\Delta_0)=0\ \longrightarrow\ J_x(s_1,s_2\,|\,\boldsymbol{k},\Delta_0)=\text{const}\,. \tag{20}$$

This implies that even under a non-uniform potential $V(x)$, such as a potential barrier, the total current across the barrier must be conserved. This unique feature plays a crucial role in electron tunneling and transmission calculation. For our considered system, we always assume a translational symmetry along the y-direction, and then $J_y(s_1,s_2\,|\,\boldsymbol{k},\Delta_0)=$ a constant.

3. Wentzel-Kramers-Brillouin Approximation

In this Section, we aim to derive the semi-classical Wentzel-Kramers-Brillouin (WKB) approximation applied to Kek-Y graphene. We begin with the Hamiltonian in Equation (1) and generalize it for the case with a spatially non-uniform potential $V(x)$ including the special case with a square barrier $V(x)=\Theta(x)\,\Theta(W_B-x)$, where W_B is the width of a square barrier.

By taking into account the fact that our system is no longer translationally invariant in the x-direction, we take $k_x\to -i\,\partial/\partial x$ and get from Equation (1) that

$$\mathcal{H}_Y(x,k_y\,|\,\Delta_0)=i\,v_F\left[\begin{array}{cc|cc} V(x) & -\hbar\,\partial/\partial x-p_y & \Delta_0(-\hbar\,\partial/\partial x-p_y) & 0 \\ -\hbar\,\partial/\partial x-k_y & V(x) & 0 & \Delta_0(-\hbar\,\partial/\partial x-p_y) \\ \hline \Delta_0(-\hbar\,\partial/\partial x+p_y) & 0 & V(x) & -\hbar\,\partial/\partial x+p_y \\ 0 & \Delta_0(-\hbar\,\partial/\partial x+p_y) & -\hbar\,\partial/\partial x-p_y & V(x) \end{array}\right], \tag{21}$$

which is independent of y, where $p_y=\hbar k_y=$ const remains conserved.

The key idea of the WKB approximation originates from a series expansion in powers of a small parameter $\hbar$. Since we will consider a semi-classical particle with a large kinetic energy $\varepsilon(k)$, it is necessary to estimate the order of magnitude for each of the considered quantities. By following Refs. [43,45], it is reasonable to rewrite the Hamiltonian in Equation (21), as well as the corresponding eigenvalue equation, in a form with only dimensionless quantities, i.e.,

$$x\longrightarrow\frac{x}{W_B}\equiv\xi\quad\text{and}\quad\varepsilon(k)\longrightarrow\frac{\varepsilon(k)}{V_0}\,, \tag{22}$$

Preprints (www.preprints.org) | NOT PEER-REVIEWED | Posted: 27 April 2023 doi:10.20944/preprints202304.1054.v1

where V_0 represents the strength of a potential, e.g., the height of a square-barrier potential. Correspondingly, we also introduce other dimensionless quantities, such as

$$V(x) \longrightarrow \frac{V(x)}{V_0} \quad \text{and} \quad p_y \longrightarrow \frac{v_F\, p_y}{V_0}\,. \tag{23}$$

In this way, the spatial derivative now becomes

$$\partial/\partial x \to \partial/(W_B\, \partial\xi)\,. \tag{24}$$

Such a scheme allows us to modify the Planck constant $\hbar$, which is our chosen small parameter for a series expansion, leading to

$$\hbar \to \left(\frac{v_F}{W_B V_0}\right) \hbar\,, \tag{25}$$

Consequently, the new energy scale of an incoming particle is large and will not be limited by the Fermi energy of electrons in graphene.

In this study, we follow an established WKB solution for a Dirac equation and expand our sought after wave function as a series, given by

$$\begin{aligned} \Psi_Y(s_1,s_2\,|\,x,k_y) &= \exp\left[\frac{i}{\hbar_0}\,\mathbb{S}(x)\right] \sum_{\lambda=0}^{\infty} (-i\hbar_0)^{\lambda}\, \Psi_\lambda(x,k_y) \\ &= \exp\left[\frac{i}{\hbar_0}\,\mathbb{S}(x)\right] \left[\Psi_0(x,k_y) - i\hbar_0\, \Psi_1(x,k_y) - \hbar_0^2\, \Psi_2(x,k_y) + \cdots\right]\,, \end{aligned} \tag{26}$$

where $\mathbb{S}(x)$ stands for a semi-classical action in the WKB approximation. Here, our goal is finding a differential equation with respect to x, which connects consecutive terms in the expansion introduced in Equation (26). Explicitly, we would seek the form

$$\hat{\mathbb{D}}_x^{(4)}(\Delta_0)\left[\frac{\partial}{\partial x}\,\Psi_\lambda(s_1,s_2\,|\,x,k_y)\right] - \hat{\mathbb{O}}_T(s_1,s_2\,|\,x,p_y,\Delta_0)\,\Psi_{\lambda+1}(s_1,s_2\,|\,x,k_y) = 0\,, \tag{27}$$

where

$$\begin{aligned} \hat{\mathbb{D}}_x^{(4)}(\Delta_0) &= \hat{\mathcal{T}}_0^{(2)} \otimes \hat{\Sigma}_x^{(2)} + \Delta_0\, \hat{\mathcal{T}}_x^{(2)} \otimes \hat{\Sigma}_0^{(2)} \\ &= \left[\begin{array}{cc|cc} 0 & 1 & \Delta_0 & 0 \\ 1 & 0 & 0 & \Delta_0 \\ \hline \Delta_0 & 0 & 0 & 1 \\ 0 & \Delta_0 & 1 & 0 \end{array}\right] \end{aligned} \tag{28}$$

is proportional to the probability-current operator in Equation (17), $\lambda = 0, 1, 2, 3, \cdots$, and $\Psi_{\lambda=-1}(s_1,s_2\,|\,x,k_y) \equiv 0$. Furthermore, the transport operator $\hat{\mathbb{O}}_T(s_1,s_2\,|\,x,p_y,\Delta_0)$ introduced in Equation (27), which connects each two consecutive terms of expansion in Equation (26), is

$$\begin{aligned} &\hat{\mathbb{O}}_T(s_1,s_2\,|\,x,p_y,\Delta_0) \\ &= \xi(x)\,\hat{\mathcal{T}}_0^{(2)} \otimes \hat{\Sigma}_0^{(2)} + \hat{\mathcal{T}}_0^{(2)} \otimes \left[\hat{\boldsymbol{\Sigma}}^{(2)} \cdot \left\{\frac{\partial}{\partial x}\,\mathbb{S}(x), p_y\right\}\right] + \Delta_0 \left[\hat{\boldsymbol{\mathcal{T}}}^{(2)} \cdot \left\{\frac{\partial}{\partial x}\,\mathbb{S}(x), p_y\right\}\right] \otimes \hat{\Sigma}_0^{(2)} \\ &= \left[\begin{array}{cc|cc} \xi(x) & \partial\,\mathbb{S}(x)/\partial x - ip_y & \Delta_0[\partial\,\mathbb{S}(x)/\partial x - ip_y] & 0 \\ \partial\,\mathbb{S}(x)/\partial x + ip_y & \xi(x) & 0 & \Delta_0[\partial\,\mathbb{S}(x)/\partial x - ip_y] \\ \hline \Delta_0[\partial\,\mathbb{S}(x)/\partial x + ip_y] & 0 & \xi(x) & \partial\,\mathbb{S}(x)/\partial x + ip_y \\ 0 & \Delta_0[\partial\,\mathbb{S}(x)/\partial x + ip_y] & \partial\,\mathbb{S}(x)/\partial x - ip_y & \xi(x) \end{array}\right]\,, \end{aligned} \tag{29}$$

where $\xi(x) = V(x) - \varepsilon(p_y)$.

Preprints (www.preprints.org) | NOT PEER-REVIEWED | Posted: 27 April 2023 doi:10.20944/preprints202304.1054.v1

Specifically, for $\lambda = -1$, we get

$$\hat{\mathbb{O}}_T(s_1, s_2 \,|\, x, p_y, \Delta_0)\, \Psi_0(s_1, s_2 \,|\, x, k_y) = 0\,. \tag{30}$$

For the linear homogeneous equation in Equation (30), a non-trivial solution becomes possible only if its determinant is zero, i.e.,

$$\begin{aligned}&\left[\left(\frac{\partial\,\mathbb{S}(x)}{\partial x}\right)^2 + p_y^2\right]^2 - 2\Delta_0^2\left[\left(\frac{\partial\,\mathbb{S}(x)}{\partial x}\right)^4 - p_y^4\right] + \Delta_0^4\left[\left(\frac{\partial\,\mathbb{S}(x)}{\partial x}\right)^2 + p_y^2\right]^2 \\ &-2\xi^2(x)\left[\left(\frac{\partial\,\mathbb{S}(x)}{\partial x}\right)^2 + p_y^2\right]\left(1+\Delta_0^2\right) + \xi^4(x) = 0\,.\end{aligned} \tag{31}$$

As a quartic equation, Equation (31) could be solved analytically, but in the general case its solutions are too tedious to write them down. Instead, we use the fact that $\Delta_0 \ll 1$. Therefore, as $\Delta_0 \longrightarrow 0$, Equation (31) turns into

$$\left[\left(\frac{\partial\,\mathbb{S}(x)}{\partial x}\right)^2 + p_y^2\right]^2 - 2\left[\left(\frac{\partial\,\mathbb{S}(x)}{\partial x}\right)^2 + p_y^2\right]\xi^2(x) + \xi^4(x) = 0 \tag{32}$$

with a set of doubly degenerate solutions for incident energy ε_0 of an electron, given by

$$p_x(x) \equiv \frac{\partial\,\mathbb{S}(x)}{\partial x} = \pm\sqrt{[\varepsilon_0 - V(x)]^2 - p_y^2}\,, \tag{33}$$

which results in

$$\mathbb{S}(x) - \mathbb{S}(x_0) = \int_{x_0}^{x} d\zeta\,\sqrt{[\varepsilon_0 - V(\zeta)]^2 - p_y^2}\,. \tag{34}$$

For a finite but small Δ_0, we are able to solve Equation (31) by using a perturbation method. Assuming

$$p_x(x) = p_x^{(0)}(x) + \Delta_0^2\, p_x^{(1)}(x) + \cdots\,, \tag{35}$$

where $p_x^{(0)}(x) = \pm\sqrt{[\varepsilon_0 - V(x)]^2 - p_y^2}$ derived from the zeroth-order equation in Equation (32), we obtain the first-order correction $p_x^{(1)}(x)$ (on the order of $\simeq \Delta_0^2$) from the following equation

$$\begin{aligned}&4\,p_x^{(0)}(x)\,p_x^{(1)}(x)\left\{\left[p_x^{(0)}(x)\right]^2 + p_y^2\right\} - 2\left\{\left[p_x^{(0)}(x)\right]^4 - p_y^2\right\} \\ &+2\left\{\left[p_x^{(0)}(x)\right]^2 + 2p_x^{(0)}(x)\,p_x^{(1)}(x) + p_y^2\right\}\,[\varepsilon_0 - V(x)]^2 = 0\,,\end{aligned} \tag{36}$$

given by

$$p_x^{(1)}(x) = \frac{\left[p_x^{(0)}(x)\right]^4 - p_y^4 + \left[p_x^{(0)}(x)\right]^2\xi^2(x) + p_y^2\,\xi^2(x)}{2\,p_x^{(0)}(x)\left\{\left[p_x^{(0)}(x)\right]^2 + p_y^2 - \xi^2(x)\right\}}\,. \tag{37}$$

Equations (35)–(37) define the solution for the x-dependent momentum $p_x(x)$, while the semi-classical action for a given momentum $p_x(x)$ can be determined by Equation (34). This is one of the most crucial results in semi-classical theory for Kekulé-patterned graphene.

Now, the WKB wave function could be obtained from Equation (27). If we look for an eigenstate formally in the following form

$$\boldsymbol{\Psi}_{\mathrm{WKB}}(s_1, s_2 \,|\, x, p_y) = \left[\begin{array}{c} \Psi_A(x) \\ \Psi_B(x) \\ \hline \Psi'_A(x) \\ \Psi'_B(x) \end{array} \right] , \tag{38}$$

the relations between its components become

$$\begin{aligned} &\xi(x)\,\Psi_A(x) + \Delta_0\,\left[p_x(x) - ip_y\right]\,\Psi'_A(x) + \left[p_x(x) - ip_y\right]\,\Psi_B(x) = 0\,, \\ &\left[p_x(x) - ip_y\right]\,\Psi_A(x) + \xi(x)\,\Psi_B(x) + \Delta_0\,\left[p_x(x) - ip_y\right]\,\Psi'_B(x) = 0\,, \\ &\Delta_0\,\left[p_x(x) + ip_y\right]\,\Psi_A(x) + \xi(x)\,\Psi'_A(x) + \Delta_0\,\left[p_x(x) - ip_y\right]\,\Psi'_B(x) = 0\,, \end{aligned} \tag{39}$$

where $p_x(x)$ is determined from Equations (35)–(37). It is important to point out that the equations in Equation (39) includes strain-induced coupling Δ_0 between two sets of wave functions $\Psi_{A,B}(x)$ and $\Psi'_{A,B}(x)$, giving rise to a similar interband probability current [75] within the semi-classical frame.

In general, the solution for a WKB wave function is quite complicated but we can model a reliable solution by using the fact that the wave functions in Kek-Y graphene is a combination of two graphene wave function and does not depend on Δ_0. For this purpose, we first introduce a notation

$$\Theta(x, p_y) = \frac{1}{\xi(x)}\,\left[\pi_x(\xi) - i\pi_y\right] = -\mathtt{exp}\left[-i\tau\,\theta_{\mathbf{k}}(x)\right]\,. \tag{40}$$

where, $\theta_{\mathbf{k}}(\xi) = \tan^{-1}[k_x(\xi)/k_y]$ is the angle between wave vector $\boldsymbol{k} = \{k_x(\xi), k_y\} = (1/\hbar)\,\{\pi_x(\xi), \pi_y\}$ and the x-axis. Making use of this notation, the wave function now takes a simple form

$$\Psi_Y(s_1, s_2 \,|\, x, p_y) = \left[\begin{array}{c} \Theta(x, p_y) \\ s_1 \\ s_2 \\ s_1 s_2\,\Theta^*(x, p_y) \end{array} \right] \varphi_H^{(0)}(x)\,. \tag{41}$$

Finally, in analogy with graphene study, we obtain the following expression

$$\varphi_H^{(0)}(x) = \left[\frac{p_x^2(x) + p_y^2}{p_x^2(x)}\right]^{1/2} = \left\{1 + \left[\frac{p_y}{p_x(x)}\right]^2\right\}^{1/2} , \tag{42}$$

and now the wave function in Equation (12) is fully determined.

Up to now, we have eventually obtained the semi-classical action in Equation (34), the x-dependent momentum $p_x(x)$, and the WKB wave function in Equation (12). This concludes constructing a semi-classical theory for Kek-Y graphene.

4. Electron tunneling in Kekulé-patterned graphene

The primary application of the obtained WKB approximation is a good numerical estimate of the electron transmission amplitude for a fast-moving electron. This method is easily applicable to the cases of non-square potential barriers and a wide class of potential profiles as long as this profile $V(x)$ is smooth and there is no abrupt change in the particle's momentum $p(x)$. At the same time, WKB calculations were used to predict or verify the existence of the Klein paradox for a normally incident particle on a square barrier in graphene and other Dirac cone materials, i.e., could be formally applied to a square barrier as well.

 doi:10.20944/preprints202304.1054.v1

The transmission amplitude is defined as the ratio of the electron current passing through the barrier to the incoming current. Since the total current in the direction perpendicular to a potential barrier is conserved, the reflect current could be also easily calculated as the difference between them. The biggest loss of a transmitted current occurs in the classically forbidden regions (CFR) in which the longitudinal momentum $p_x(x)$ becomes purely imaginary and the moving particle is represented by an evanescent wave whose amplitude is exponentially decreasing along the x-axis. The transmission amplitude $\mathbb{T}(p_y \,|\, a, \Delta_0)$ in WKB theory is estimated by the integral of the purely imaginary momentum $p_x(x)$ over each of the classically forbidden regions along the x-direction. This results in the following equation

$$\mathbb{T}(p_y \,|\, a, \Delta_0) = \texttt{exp}\left[-\frac{2}{\hbar} \int\limits_{\text{CFR}} |p_x(x)| \, dx \right] \tag{43}$$

as long as the condition $\int\limits_{\text{CFR}} |p_x(x)| \, dx \gg \hbar$ is satisfied. Based on Equation (31), squared longitudinal momentum $\Pi^{(S)}(x) = p_x^2(x)$ is determined from

$$\left[\Pi^{(S)}(x) + p_y^2\right]^2 - 2\Delta_0^2 \left\{ \left[\Pi^{(S)}(x)\right]^2 - p_y^4 \right\} - 2\left[\varepsilon_0 - V(x)\right]^2 \left[\Pi^{(S)}(x) + p_y^2\right] \left(1 + \Delta_0^2\right) + \left[\varepsilon_0 - V(x)\right]^4 = 0\,. \tag{44}$$

The calculated locations of CFRs are presented in Figure 3 for $\Delta_0 = 0$ and in Figure 4 for $\Delta_0 \neq 0$. We see that the former case is pretty much equivalent to graphene and the boundaries of the CFR's are linear and symmetric with respect to $x = 0$. The width of the classically inaccessible region along the x-axis obviously depends on the slope of the potential profile, i.e., a higher slope a corresponds to reduced width of a CFR.

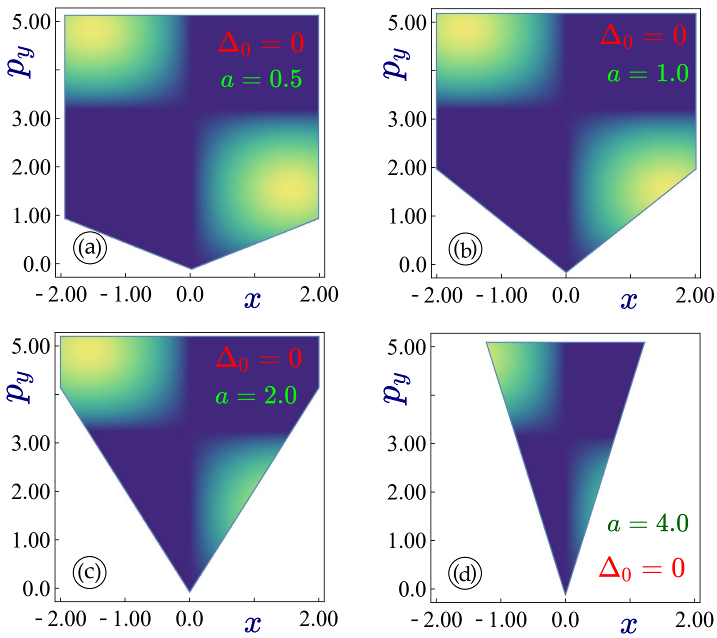

Figure 3. (Color online) Regions for the classically forbidden (or classically inaccessible regions) with $\text{Im}\,[p_x(x)] \neq 0$ for an incoming electron with a linear potential $V(x) = ax$. Here, we select a crossing point, corresponding to the electron-to-hole (and back) state transition $\varepsilon_Y(s_1, s_2 \,|\, k, \Delta_0) = 0$ at $x = 0$. All panels (**a**–**d**) are calculated for $\Delta_0 = 0$ but different values of a.

Preprints (www.preprints.org) | NOT PEER-REVIEWED | Posted: 27 April 2023 doi:10.20944/preprints202304.1054.v1

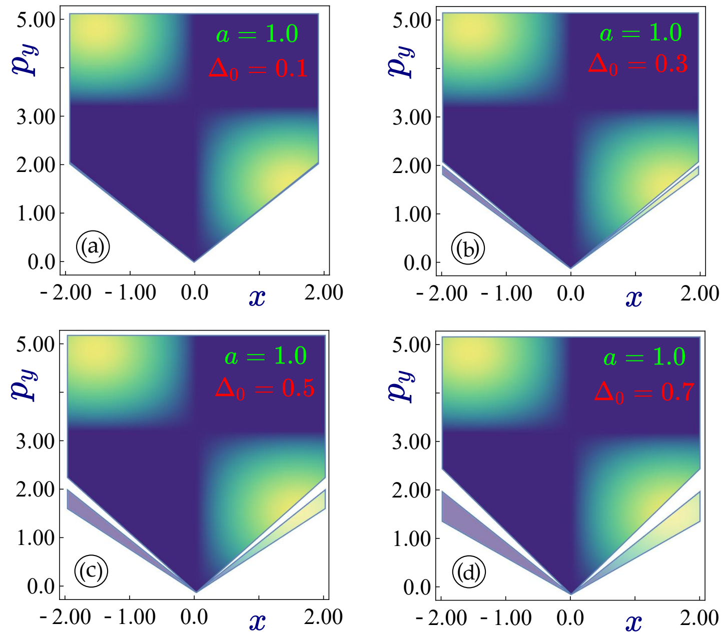

Figure 4. (Color online) Regions for the classically forbidden (or classically inaccessible regions) with $\mathrm{Im}\,[p_x(x)] \neq 0$ for an incoming electron with a linear potential $V(x) = ax$. Here we select a crossing point, corresponding to the electron-to-hole (and back) state transition $\varepsilon_Y(s_1, s_2 \,|\, k, \Delta_0) = 0$ at $x = 0$. Panels (**a**–**d**) are calculated with $a = 1$ and various finite values of Δ_0.

When $\Delta_0 \neq 0$, the equation with classically forbidden regions is much more complicated and the region itself is extended in a non-trivial way, as seen from Figure 4. However, the boundaries of CFR are still linear and symmetric with respect to $x = 0$. This is in stark contrast with gapped α-$\mathcal{T}_3$ materials in which the classically inaccessible regions are very complicated, asymmetric and even involve curved boundaries.

Our results for the transmission are presented in Figure 5. First, we find that the expansion of the classical and accessible region leads to lower transmission so that it is more suppressed for a smaller slope a in the potential profile $V(x)$, as found from Figure 5a. Similarly, the suppression of transmission $\mathbb{T}(p_y \,|\, a, \Delta_0)$ increases for a finite Δ_0 due to the appearance of extended CFRs, However, its dependence on Δ_0 is much smaller compared to that on the potential profile slope a, as can be verified by Figure 5a.

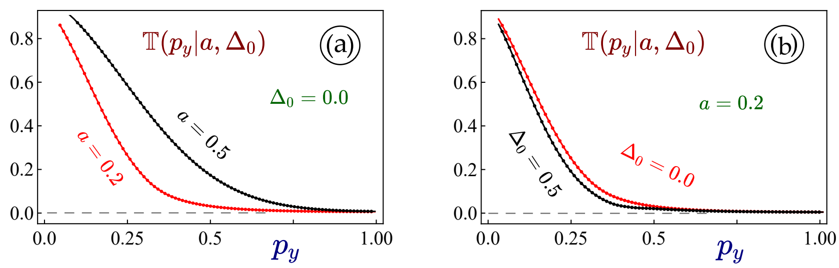

Figure 5. (Color online) Transmissions amplitudes $\mathbb{T}\left(p_y \,|\, a, \Delta_0\right)$ calculated by using Equation (43). Panel (**a**) presents $\mathbb{T}\left(p_y \,|\, a, \Delta_0\right)$ as a function of transverse momentum p_y for $\Delta_0 = 0$ and different slopes $a = 0.2$ and 0.5. Panel (**b**) displays calculated $T\left(p_y \,|\, a, \Delta_0\right)$ as a function of p_y for $a = 0.2$ and different energy gaps $\Delta_0 = 0$ and 0.5.

It is important to mention that the WKB approximation provides a fairly satisfactory estimate for the electron transmission in the cases as standard techniques are either not applicable or would lead to tremendously complicated equations. This is exactly the case for Kek-Y graphene in which similarly to tunneling of Rashba electrons there are two non-equivalent solutions for wave vector k at a given energy [76]. However, in the case of Kek-Y graphene, we would need solve a quartic equation so as to obtain the k value for a given energy ε_0, and then use these expressions to find transmission which seems hardly possible.

5. Concluding remarks

In conclusion, we have built a complete semi-classical WKB theory for recently discovered Kek-Y patterned graphene with two coupled gapless Dirac cones with different Fermi velocities $v_F(1 \pm \Delta_0)$. This includes finding the semi-classical action, x-dependent longitudinal momentum $p_x(x)$ and leading-order WKB wave function. Meanwhile, we have also derived and solved the transport equation which connects every two successive orders of a sought wave function.

Our obtained WKB equations are further applied to calculate the electron transmission amplitudes based on classically inaccessible regions. We have demonstrated that the slope a of a linear potential $V(x) = ax$ can strongly affect electron transmission, while the coupling parameter Δ_0 has a very limited effect on transmission because it only slightly modifies the location and size of a classically forbidden region for a specified incoming electron.

Based on the present study, we are strongly convinced that this work reveals a crucial step in advancing our knowledge on the electronic properties of newly discovered Dirac materials. Our obtained WKB theory provides a powerful tool for systematically investigating crucial electronic and transport properties of novel Dirac materials, which have numerous applications in modern electronic and opto-electronic devices, and especially in valleytronics.

Acknowledgments: A.I. would like to acknowledge the funding received from TRADA-53-130 PSC-CUNY Award 65094-00 53. D.H. was supported by the Air Force Office of Scientific Research (AFOSR). G.G. would like to acknowledge Grant No. FA9453-21-1-0046 from the Air Force Research Laboratory (AFRL).

References

1. OV Gamayun, VP Ostroukh, NV Gnezdilov, İnanç Adagideli, and CWJ Beenakker. Valley-momentum locking in a graphene superlattice with y-shaped kekulé bond texture. *New Journal of Physics*, 20(2):023016, 2018.
2. Yawar Mohammadi. Electronic spectrum and optical properties of y-shaped kekulé-patterned graphene: Band nesting resonance as an optical signature. *ECS Journal of Solid State Science and Technology*, 11(12):121004, 2022.
3. Saúl A Herrera and Gerardo G Naumis. Electronic and optical conductivity of kekulé-patterned graphene: Intravalley and intervalley transport. *Physical Review B*, 101(20):205413, 2020.
4. Christopher Gutiérrez, Cheol-Joo Kim, Lola Brown, Theanne Schiros, Dennis Nordlund, Edward B Lochocki, Kyle M Shen, Jiwoong Park, and Abhay N Pasupathy. Imaging chiral symmetry breaking from kekulé bond order in graphene. *Nature Physics*, 12(10):950–958, 2016.
5. Alexis Coissard, David Wander, Hadrien Vignaud, Adolfo G Grushin, Cécile Repellin, Kenji Watanabe, Takashi Taniguchi, Frédéric Gay, Clemens B Winkelmann, Hervé Courtois, et al. Imaging tunable quantum hall broken-symmetry orders in graphene. *Nature*, 605(7908):51–56, 2022.
6. Xiao Yan Xu, Kam Tuen Law, and Patrick A Lee. Kekulé valence bond order in an extended hubbard model on the honeycomb lattice with possible applications to twisted bilayer graphene. *Physical Review B*, 98(12):121406, 2018.
7. Elias Andrade, Ramon Carrillo-Bastos, and Gerardo G Naumis. Valley engineering by strain in kekulé-distorted graphene. *Physical Review B*, 99(3):035411, 2019.
8. Elias Andrade, Ramon Carrillo-Bastos, Mahmoud M Asmar, and Gerardo G Naumis. Kekulé-induced valley birefringence and skew scattering in graphene. *Physical Review B*, 106(19):195413, 2022.
9. Elías Andrade, Gerardo G Naumis, and Ramon Carrillo-Bastos. Electronic spectrum of kekulé patterned graphene considering second neighbor-interactions. *Journal of Physics: Condensed Matter*, 33(22):225301, 2021.
10. MA Mojarro, VG Ibarra-Sierra, JC Sandoval-Santana, R Carrillo-Bastos, and Gerardo G Naumis. Dynamical floquet spectrum of kekulé-distorted graphene under normal incidence of electromagnetic radiation. *Physical Review B*, 102(16):165301, 2020.
11. Andre Konstantin Geim. Graphene: status and prospects. *science*, 324(5934):1530–1534, 2009.

 doi:10.20944/preprints202304.1054.v1

12. AH Castro Neto, Francisco Guinea, Nuno MR Peres, Kostya S Novoselov, and Andre K Geim. The electronic properties of graphene. *Reviews of modern physics*, 81(1):109, 2009.
13. Michel Houssa, A Dimoulas, and A Molle. Silicene: a review of recent experimental and theoretical investigations. *Journal of Physics: Condensed Matter*, 27(25):253002, 2015.
14. Abdelkader Kara, Hanna Enriquez, Ari P Seitsonen, LC Lew Yan Voon, Sébastien Vizzini, Bernard Aufray, and Hamid Oughaddou. A review on silicene—new candidate for electronics. *Surface science reports*, 67(1):1–18, 2012.
15. Motohiko Ezawa. A topological insulator and helical zero mode in silicene under an inhomogeneous electric field. *New Journal of Physics*, 14(3):033003, 2012.
16. Wonbong Choi, Nitin Choudhary, Gang Hee Han, Juhong Park, Deji Akinwande, and Young Hee Lee. Recent development of two-dimensional transition metal dichalcogenides and their applications. *Materials Today*, 20(3):116–130, 2017.
17. Sajedeh Manzeli, Dmitry Ovchinnikov, Diego Pasquier, Oleg V Yazyev, and Andras Kis. 2d transition metal dichalcogenides. *Nature Reviews Materials*, 2(8):1–15, 2017.
18. Calvin Tabert. *Electronic Phenomena in 2D Dirac-like Systems: Silicene and Topological Insulator Surface States*. PhD thesis, University of Guelph, 2015.
19. Emilia Illes. *Properties of the α-T3 Model*. PhD thesis, University of Guelph, 2017.
20. D Bercioux, DF Urban, Hermann Grabert, and Wolfgang Häusler. Massless dirac-weyl fermions in a t 3 optical lattice. *Physical Review A*, 80(6):063603, 2009.
21. Andrii Iurov, Godfrey Gumbs, and Danhong Huang. Many-body effects and optical properties of single and double layer α-lattices. *Journal of Physics: Condensed Matter*, 32(41):415303, 2020.
22. JD Malcolm and EJ Nicol. Frequency-dependent polarizability, plasmons, and screening in the two-dimensional pseudospin-1 dice lattice. *Physical Review B*, 93(16):165433, 2016.
23. Andrii Iurov, Liubov Zhemchuzhna, Dipendra Dahal, Godfrey Gumbs, and Danhong Huang. Quantum-statistical theory for laser-tuned transport and optical conductivities of dressed electrons in α- t 3 materials. *Physical Review B*, 101(3):035129, 2020.
24. Alexander Filusch and Holger Fehske. Tunable valley filtering in dynamically strained α- t 3 lattices. *Physical Review B*, 106(24):245106, 2022.
25. Wen Zeng and Rui Shen. Pure crossed andreev reflection assisted transverse valley currents in α-t_3 lattices. *arXiv preprint arXiv:2205.14930*, 2022.
26. Fu Li, Qingtian Zhang, and Kwok Sum Chan. Novel transport properties of the α-t3 lattice with uniform electric and magnetic fields: the effects of flat bands. 2022.
27. Andrii Iurov, Godfrey Gumbs, and Danhong Huang. Temperature-and frequency-dependent optical and transport conductivities in doped buckled honeycomb lattices. *Physical Review B*, 98(7):075414, 2018.
28. Lakpa Tamang and Tutul Biswas. Probing topological signatures in an optically driven α- t 3 lattice. *Physical Review B*, 107(8):085408, 2023.
29. Andrii Iurov, Liubov Zhemchuzhna, Godfrey Gumbs, Danhong Huang, Dipendra Dahal, and Yonatan Abranyos. Finite-temperature plasmons, damping, and collective behavior in the $\alpha - \sqcup_3$ model. *Phys. Rev. B*, 105:245414, 2022.
30. Tutul Biswas and Tarun Kanti Ghosh. Dynamics of a quasiparticle in the α-t3 model: role of pseudospin polarization and transverse magnetic field on zitterbewegung. *Journal of Physics: Condensed Matter*, 30(7):075301, 2018.
31. EV Gorbar, VP Gusynin, and DO Oriekhov. Electron states for gapped pseudospin-1 fermions in the field of a charged impurity. *Physical Review B*, 99(15):155124, 2019.
32. DO Oriekhov and VP Gusynin. Optical conductivity of semi-dirac and pseudospin-1 models: Zitterbewegung approach. *Physical Review B*, 106(11):115143, 2022.
33. PO Sukhachov, DO Oriekhov, and EV Gorbar. Optical conductivity of bilayer dice lattices. *arXiv preprint arXiv:2303.08258*, 2023.
34. DO Oriekhov and VP Gusynin. Rkky interaction in a doped pseudospin-1 fermion system at finite temperature. *Physical Review B*, 101(23):235162, 2020.
35. Antonios Balassis, Dipendra Dahal, Godfrey Gumbs, Andrii Iurov, Danhong Huang, and Oleksiy Roslyak. Magnetoplasmons for the α-t3 model with filled landau levels. *Journal of Physics: Condensed Matter*, 32(48):485301, 2020.

36. Calvin J Tabert and Elisabeth J Nicol. Valley-spin polarization in the magneto-optical response of silicene and other similar 2d crystals. *Physical Review Letters*, 110(19):197402, 2013.
37. Calvin J Tabert and Elisabeth J Nicol. Magneto-optical conductivity of silicene and other buckled honeycomb lattices. *Physical Review B*, 88(8):085434, 2013.
38. Godfrey Gumbs, Andrii Iurov, Danhong Huang, and Liubov Zhemchuzhna. Revealing hofstadter spectrum for graphene in a periodic potential. *Physical Review B*, 89(24):241407, 2014.
39. Áron Dániel Kovács, Gyula Dávid, Balázs Dóra, and József Cserti. Frequency-dependent magneto-optical conductivity in the generalized α- t 3 model. *Physical Review B*, 95(3):035414, 2017.
40. A Raoux, M Morigi, J-N Fuchs, F Piéchon, and G Montambaux. From dia-to paramagnetic orbital susceptibility of massless fermions. *Physical review letters*, 112(2):026402, 2014.
41. M Vogl, O Pankratov, and S Shallcross. Semiclassics for matrix hamiltonians: The gutzwiller trace formula with applications to graphene-type systems. *Physical Review B*, 96(3):035442, 2017.
42. Yuhui Zhang, Yafis Barlas, and Kun Yang. Coulomb impurity under magnetic field in graphene: A semiclassical approach. *Physical Review B*, 85(16):165423, 2012.
43. Nicholas Weekes, Andrii Iurov, Liubov Zhemchuzhna, Godfrey Gumbs, and Danhong Huang. Generalized wkb theory for electron tunneling in gapped α- t 3 lattices. *Physical Review B*, 103(16):165429, 2021.
44. VV Zalipaev, DN Maksimov, CM Linton, and FV Kusmartsev. Spectrum of localized states in graphene quantum dots and wires. *Physics Letters A*, 377(3-4):216–221, 2013.
45. V Zalipaev, CM Linton, MD Croitoru, and A Vagov. Resonant tunneling and localized states in a graphene monolayer with a mass gap. *Physical Review B*, 91(8):085405, 2015.
46. Kathy Blaise, Chinedu Ejiogu, Andrii Iurov, Liubov Zhemchuzhna, Godfrey Gumbs, and Danhong Huang. Developing semiclassical wentzel-kramers-brillouin theory for α- t 3 model. *Physical Review B*, 107(4):045128, 2023.
47. VV Zalipaev. Complex wkb approximations in graphene electron-hole waveguides in magnetic field. *GRAPHENE–SYNTHESIS, CHARACTERIZATION, PROPERTIES AND APPLICATIONS*, page 81, 2011.
48. Juan Juan Wang, S Liu, J Wang, and Jun-Feng Liu. Valley-coupled transport in graphene with y-shaped kekulé structure. *Physical Review B*, 98(19):195436, 2018.
49. Elias Andrade, Ramon Carrillo-Bastos, Pierre A Pantaleon, and Francisco Mireles. Resonant transport in kekule-distorted graphene nanoribbons. *Journal of Applied Physics*, 127(5):054304, 2020.
50. MI Katsnelson, KS Novoselov, and AK Geim. Chiral tunnelling and the klein paradox in graphene. *Nature physics*, 2(9):620–625, 2006.
51. Pierre E Allain and Jean-Noel Fuchs. Klein tunneling in graphene: optics with massless electrons. *The European Physical Journal B*, 83:301–317, 2011.
52. Godfrey Gumbs, Antonios Balassis, Andrii , and Paula Fekete. Strongly localized image states of spherical graphitic particles. *The Scientific World Journal*, 2014, 2014.
53. O Roslyak, A Iurov, Godfrey Gumbs, and Danhong Huang. Unimpeded tunneling in graphene nanoribbons. *Journal of Physics: Condensed Matter*, 22(16):165301, 2010.
54. Andrii Iurov, Liubov Zhemchuzhna, Godfrey Gumbs, Danhong Huang, Paula Fekete, Farhana Anwar, Dipendra Dahal, and Nicholas Weekes. Tailoring plasmon excitations in α-t 3 armchair nanoribbons. *Scientific reports*, 11(1):20577, 2021.
55. E Illes and EJ Nicol. Klein tunneling in the α- t 3 model. *Physical Review B*, 95(23):235432, 2017.
56. Xin Ye, Sha-Sha Ke, Xin-Wei Du, Yong Guo, and Hai-Feng Lü. Quantum tunneling in the α-t 3 model with an effective mass term. *Journal of Low Temperature Physics*, 199(5-6):1332–1343, 2020.
57. SM Cunha, DR da Costa, J Milton Pereira Jr, RN Costa Filho, B Van Duppen, and FM Peeters. Tunneling properties in α- t 3 lattices: Effects of symmetry-breaking terms. *Physical Review B*, 105(16):165402, 2022.
58. L Mandhour and F Bouhadida. Klein tunneling in deformed α-t_3 lattice. *arXiv preprint arXiv:2004.10144*, 2020.
59. Andrii Iurov, Liubov Zhemchuzhna, Paula Fekete, Godfrey Gumbs, and Danhong Huang. Klein tunneling of optically tunable dirac particles with elliptical dispersions. *Physical Review Research*, 2(4):043245, 2020.
60. Zhenglu Li, Ting Cao, Meng Wu, and Steven G Louie. Generation of anisotropic massless dirac fermions and asymmetric klein tunneling in few-layer black phosphorus superlattices. *Nano letters*, 17(4):2280–2286, 2017.
61. Andrii Iurov, Liubov Zhemchuzhna, Godfrey Gumbs, Danhong Huang, and Paula Fekete. Optically modulated tunneling current of dressed electrons in graphene and a dice lattice. *Physical Review B*, 105(11):115309, 2022.

62. M Barbier, P Vasilopoulos, and FM Peeters. Extra dirac points in the energy spectrum for superlattices on single-layer graphene. *Physical Review B*, 81(7):075438, 2010.
63. Andrii Iurov, Godfrey Gumbs, and Danhong Huang. Peculiar electronic states, symmetries, and berry phases in irradiated α- t 3 materials. *Physical Review B*, 99(20):205135, 2019.
64. OV Kibis. Metal-insulator transition in graphene induced by circularly polarized photons. *Physical Review B*, 81(16):165433, 2010.
65. Michael Barbier, Panagiotis Vasilopoulos, and Francois M Peeters. Single-layer and bilayer graphene superlattices: collimation, additional dirac points and dirac lines. *Philosophical Transactions of the Royal Society A: Mathematical, Physical and Engineering Sciences*, 368(1932):5499–5524, 2010.
66. J Milton Pereira, FM Peeters, A Chaves, and GA Farias. Klein tunneling in single and multiple barriers in graphene. *Semiconductor science and technology*, 25(3):033002, 2010.
67. Bashab Dey and Tarun Kanti Ghosh. Floquet topological phase transition in the α- t 3 lattice. *Physical Review B*, 99(20):205429, 2019.
68. Andrii Iurov, Godfrey Gumbs, and Danhong Huang. Exchange and correlation energies in silicene illuminated by circularly polarized light. *Journal of Modern Optics*, 64(9):913–920, 2017.
69. Andrii Iurov, Liubov Zhemchuzhna, Godfrey Gumbs, and Danhong Huang. Exploring interacting floquet states in black phosphorus: Anisotropy and bandgap laser tuning. *Journal of Applied Physics*, 122(12):124301, 2017.
70. IV Iorsh, DA Zezyulin, SA Kolodny, RE Sinitskiy, and OV Kibis. Floquet engineering of excitons in semiconductor quantum dots. *Physical Review B*, 105(16):165414, 2022.
71. Kristinn Kristinsson, Oleg V Kibis, Skender Morina, and Ivan A Shelykh. Control of electronic transport in graphene by electromagnetic dressing. *Scientific reports*, 6(1):1–7, 2016.
72. Lakpa Tamang, Tanay Nag, and Tutul Biswas. Floquet engineering of low-energy dispersions and dynamical localization in a periodically kicked three-band system. *Physical Review B*, 104(17):174308, 2021.
73. Andrii Iurov, Liubov Zhemchuzhna, Godfrey Gumbs, Danhong Huang, Wang-Kong Tse, Kathy Blaise, and Chinedu Ejiogu. Floquet engineering of tilted and gapped dirac bandstructure in $1t'$-mos_2. *Scientific Reports*, 12(1):21348, 2022.
74. Farhana Anwar, Andrii Iurov, Danhong Huang, Godfrey Gumbs, and Ashwani Sharma. Interplay between effects of barrier tilting and scatterers within a barrier on tunneling transport of dirac electrons in graphene. *Physical Review B*, 101(11):115424, 2020.
75. Po-Hsin Shih, Godfrey Gumbs, Danhong Huang, Andrii Iurov, and Yonatan Abranyos. Blocked electron transmission/reflection by coupled rashba–zeeman effects for forward and backward spin filtering. *Journal of Applied Physics*, 132(15):154302, 2022.
76. Yee Sin Ang, Zhongshui Ma, and C Zhang. Chiral-like tunneling of electrons in two-dimensional semiconductors with rashba spin-orbit coupling. *Scientific reports*, 4(1):1–7, 2014.